Geographic Object-Oriented Analysis of UAV Multispectral Images for Tree Distribution Mapping in Mangroves

Luis Americo Conti *, Roberto Lima Barcellos, Priscila Oliveira, Francisco Cordeiro Nascimento-Neto, Marilia Cunha-Lignon

Posted Date: 8 August 2024

doi: 10.20944/preprints202408.0539.v1

Keywords: Coastal Ecosystem; UAVs; Brazil; Remote Sensing; Machine Learning; Spatial data modelling

Article

Geographic Object-Oriented Analysis of UAV Multispectral Images for Tree Distribution Mapping in Mangroves

Luis Américo Conti [1,*], Roberto Lima Barcellos [2], Priscila Oliveira [1], Francisco Cordeiro Nascimento Neto [2] and Marília Cunha-Lignon [3,4]

[1] Scola de Artes Ciências e Humanidades - Universidade de São Paulo – USP – Brazil; priscilalmoliveira@usp.br

[2] Departamento de Oceanografia - Universidade Federal de Pernambuco – UFPE- Brazil; roberto.barcellos@ufpe.br; francisco.cordeiro@ufpe.br

[3] Universidade Estadual Paulista- Campus Registro – UNESP- Brazil; cunha.lignon@unesp.br

[4] The International Union for Conservation of Nature Mangrove Specialist Group - IUCN MSG

* Correspondence: - email - lconti@usp.br Escola de Artes Ciências e Humanidades, Universidade de São Paulo. Rua Arlindo Béttio, 1000 - Ermelino Matarazzo, São Paulo - SP, 03828-000 - Brazil

Abstract: Mangroves are critical ecosystems providing essential environmental services, making their conservation crucial. High-resolution remote sensing, particularly through unmanned aerial vehicles (UAVs), offers unprecedented resolution in ecosystem mapping. This study utilizes a multispectral sensor mounted on a UAV to map mangroves at Cardoso Island on Brazil's southeastern coast and Suape on the northeastern coast. Using Geographic Object-Based Image Analysis (GEOBIA) for segmentation and classification, we employed machine learning algorithms to classify the primary mangrove species: Laguncularia racemosa, Rhizophora mangle, and Avicennia schaueriana. Two flight altitudes were used: a higher altitude for broad-scale mapping and a lower altitude for classification training, supplemented by field measurements for calibration. This method enabled the precise delineation of tree crowns and provided insights into species distribution and zonation, influenced by the distinct estuarine conditions of tides and sediment input. The high-resolution mapping achieved in this study enhances detailed analyses of mangroves, improving ecological models and biophysical estimations such as biomass and blue carbon stocks. This work highlights the potential of UAV-based multispectral imaging in advancing mangrove research and conservation efforts.

Keywords: coastal ecosystem; UAVs; Brazil; remote sensing; machine learning; spatial data modelling

1. Introduction

Mangrove ecosystems provide a diverse range of ecological services that hold significant value for local communities and global human populations (Schwenke & Heffer, 2021). These include food production, climate regulation, erosion mitigation, sediment retention, protection against wind and storms, shoreline stabilization, dune anchoring, carbon sequestration and storage, pollination, biodiversity conservation, biomass exportation, and cultural benefits such as recreation, ecotourism, and landscape preservation [2,3]. Recent findings suggest that mangroves contribute approximately $42 billion annually to global fisheries. They store an impressive 25.5 million tons of carbon each year and offer flood protection to over 15 million people [4,5].

Drones, or Uncrewed Aerial Vehicles (UAVs), are used for data gathering in many domain, particularly for mapping coastal ecosystems like mangroves, forests, and dune plants [6,7]. With sensors like multispectral cameras and LIDAR, these devices capture clear images, providing insights into land coverage and plant formations. In mangrove research, UAVs offer more adaptability than traditional satellite remote sensing due to their altitude and viewing flexibility . Such attributes are key for identifying conservation areas, monitoring ecological changes, and assessing human impacts [9].

 doi:10.20944/preprints202408.0539.v1

Recent years have seen a surge in studies validating the use of UAVs equipped with optical sensors for mapping mangrove coverage. Examples include the works of [10–18] among others. These studies collectively affirm the advantages of UAVs in this context, especially when combining optical sensors with digital surface (canopy) models. This integrated approach has been shown to yield significantly more accurate results in mapping mangrove areas compared to traditional satellite imaging methods.

Additionally, the use of UAV imagery processing has become increasingly important in accurately determining mangrove forest biophysical parameters like Aboveground Biomass (AGB), Volume, Leaf Area Index (LAI), and Blue Carbon (BC) stocks, offering a more efficient and precise method for ecological assessment [3,19–21]. These parameters were traditionally gauged through direct, labor-intensive, and time-consuming inventory methods. The current methods build on the premise that allometric equations can be used to estimate biomass from UAV-measurable parameters, such as canopy height and mangrove area. This approach utilizes supervised regression or machine learning techniques, and these are validated against field data from plot measurements or individual trees. Contributions in this field include studies by [22–25], which exemplify the effectiveness of these techniques.

In contrast, while research on mapping cover or determining the biophysical parameters of mangrove forests is well-documented, there is a lack of studies that utilize unmanned aerial vehicles (UAVs) for the detailed structural characterization of forests at the level of individual trees. This includes understanding the occurrence and distribution of species within dense and heterogeneous areas. Achieving this requires the application of Geographic Object-Based Image Analysis (GEOBIA) that operates through two intertwined stages:1- individual trees segmentation where meaningful “geo-objects” defined by grouping neighbouring pixels with analogous spectral and spatial attributes as crown polygons and 2- classification where each segmented object is allocated to predetermined classes (species) using machine learning algorithms, drawing upon their spectral, textural, spatial, and topological attributes [26].

Although some studies have already successfully applied this kind of approach (see for example [27], some methodological aspects remain still open, for example: 1- determining which tree segmentation algorithms most effectively represent "Tree Objects”, 2- understanding the optimal balance between scales and resolutions in UAV imagery (particularly how the survey altitude influences resolution and affects the discrimination of tree species). 3- ascertaining the ideal quantity of training samples required for accurate classifications. 4 - Understand how unique spectral and textural patterns allow for the individual identification of species across various locations, particularly when they grow under differing environmental conditions (such as sediment characteristics and climatological settings)

The objective of this article is to introduce a framework for segmenting and classifying mangrove trees using multispectral imagery captured by unmanned aerial vehicles (UAV) in two distinct regions along the Brazilian Coast, specifically in São Paulo and Pernambuco States. This study includes detailed experiments in data acquisition and image processing, which could provide optimization of fine-scale mapping of mangrove forests, thereby contributing significantly to conservation and monitoring efforts.

2. Materials and Methods

2.1. Study Areas

The work was carried out in two target areas in Brazil: in the state of Pernambuco, on the northeast coast (Suape Estuarine Bay) and in the state of São Paulo, on the southeast coast (Cardoso Island – Cananeia/Iguape Estuarine Lagoon System CIELS). The target areas were chosen based on a combination of factors, including their similarities: a) target areas with similar dimensions; b) associated with protected inland estuarine environments; c) where specific problems have already been recognized by previous studies, with access to abundant pre-established data and information related to ongoing or previous research projects; and d) with relatively easy access and infrastructure for surveys and fieldwork; and differences: a) located in different coastal settings (tropical-

 doi:10.20944/preprints202408.0539.v1

mesotidal/subtropical-microtidal); b) with different levels of environmental conservation and management policies.

The Cardoso Island mangrove area is in the Cananéia-Iguape Estuarine -Lagoonal System (CIELS) (Figure 1), on the border between the state of São Paulo and the state of Paraná, in southeastern Brazil. CIELS is formed by the confluence of three estuarine-lagoonal channels (Mar Pequeno, Cananéia and Cubatão), forming a bay-shaped body of water locally known as Trapandé Bay. The region is very important for containing the best-preserved coastal forest in the southeast of Brazil. This plain is surrounded by crystalline rocks of the granite complexes known as Serra do Mar [28–31]. With an approximate length of 33 km and a width of between 0.5 km and 13.0 km; within the CIELS, the Cardoso Island State Park was created in 1962 and has an area of 22,500 ha, containing more than a third of the remaining forest in the state of São Paulo. As the largest continuous region of the Atlantic Forest biome in the state, much of the park's biodiversity is made up of mangroves [32]. The region has been listed as World Heritage Sites by the United Nations Educational, Scientific and Cultural Organization (UNESCO) since 1999.

The studied site is the Perequê River subtropical mangrove (25°04'S; 47°54'W), a mangrove fragment on the northern part of Cardoso Island drained by the approximately 9.5km-long coastal river and is characterized by a semi-diurnal meso-tidal regime, with spring tides presenting an average range of 1.2m [31]. The climate is humid subtropical (2269mm/21.3°C of mean pluvial and temperature), Cwa according to Köppen classification, presenting a humid rainy season in the summer (Dec-Mar). This site is among the most extensively researched mangrove area within the CIELS, with notable studies by [32,33]. The predominant mangrove species here encompass the red mangrove (Rhizophora mangle), white mangrove (Laguncularia racemosa), and black mangrove (Avicennia schaeriana). Hibiscus pernamburcensis is found in dry transition zones, while Spartina alterniflora occupies the mangrove fringe. Basin areas are typically ruled by R. mangle and A. schaueriana, presenting diminished structural growth due to infrequent flooding, sandy substrate.

Figure 1. Location of the study area of the Cardoso Island mangrove area, south coast of the state of São Paulo - Brazil.

The estuarine bay of Suape (8°22'S; 34°57'W) is located about 40 km south of Recife (Pernambuco-Brazil) and is formed by the association of the estuaries of the coastal rivers Massangana and Tatuoca, which flow into this bay (Figure 2). The studied mangrove is situated near the mouth of a tidal channel, which drains the southern face of the Santo Agostinho granite and volcanic complex,

 doi:10.20944/preprints202408.0539.v1

eventually merging with the lower estuary of the Massangana River/Suape Bay [34]. The area experiences a semi-diurnal meso-tidal regime, boasting with tidal amplitudes of 0.97 m for neap tides and 2.07 m for spring tides. The climate in the Suape bay area is tropical hot and humid (2000mm/25.0°C of mean pluvial and temperature), As' type according to Köppen classification, with a humid rainy season in the autumn-winter, distributed from March to August [35].

The lagoon-estuary region has been seriously impacted by the construction of the Suape Industrial and Port Complex through physical and structural modifications caused by industrialization and disorderly population growth. According to [36,37], the main impacting processes in Suape are related to sedimentation dredging; siltation/erosion; reef blasting; landfills on the reef, mangrove and coastal plain; large vessel traffic; and industrial and domestic effluent discharges. The latter are the main sources of contamination of water and sediments with heavy metals [34,38] and organic pollutants, which has significantly affected the Suape mangrove areas [39].

Braga et al. (1989) described four species in the region: R. mangle, L. racemosa, with sparse occurrence of A. schauerianna and A. germinans, without a defined zonation. A fifth species, Conocarpus erectus, occurred only in the mangrove-dune transition. There is a notable predominance of R. mangle and L. racemosa occurring in the region and no occurrence of the genus Avicennia was recorded in the specific region of the study area.

Figure 2. the study area of the Suape Bay mangrove area, south coast of the state of Pernambuco - Brazil.

2.2. Uncrewed Aerial Vehicle (UAV) Imaging

The surveys were carried out using the DJI Phantom P4 drone with Multispectral sensor (P4M). The P4M has a total of six image sensors, including a visible light camera (RGB) and five multispectral cameras, blue (B - 450-475 nm), green (G - 515-595 nm), red (R - 640-670 nm), red edge (RE - 725-775 nm) and near infrared (NIR - 840-890 nm). The focal length of the P4M camera is 5.74 mm, the image size is 1600 × 1300 pixels, and the sensor size is 4.87 mm × 3.96 mm (LU et al., 2020). The equipment has an on-board radiometer that compensate and equalize the brightness of the images. The flights were planned employing using the DJI GS PRO application at a speed of 1.4 m/s with 80% lateral and longitudinal overlap. Flights were made at an altitude of 100-meter (mapping flights) considered ideal for mapping purposes (pixel ~6,2 cm) and the 30-meter flights for detailing and species recognition (pixel ~ 1.4 cm), as they proved to be suitable to differentiate the species in our research.

 doi:10.20944/preprints202408.0539.v1

The Suape mangrove flights were performed on April 29, 2022. While the Cardoso Island mangrove flight was acquired on September 20, 2022. Both flights were carried out in the morning with low tide conditions partly cloudy weather and no winds that could interfere with the flight plan. For Suape mangrove, the imaging flight generated 2987 photos, covering a total area of 31 ha and a total of 588 images over an area of 1.31 ha for the detail flight. In the case of Cardoso Island, the mapping flight generated 2870 photos for an area of 36.01 ha and the sum of the detailing flights generated 2002 images for an area of 0.83 ha.

The UAV imagery was processed using the 'Structure from Motion (SfM)' methodology in the PIX4D Mapper software [41]. This technique, rooted in the foundational principles of stereoscopic photogrammetry, leverages geometric attributes from an array of images captured at different angular orientations. This created a sparse point cloud, established through the consistent identification of salient features across various images. This orientation ensured that each photograph was aligned relative to shared, identifiable points, streamlining the data processing stage.

Subsequently, a dense dense point cloud was derived by correlating congruent pixel sets from the initially aligned images. Using this dense data structure, 3D spatial models were crafted utilizing the Scale Invariant Feature Transform (SIFT) algorithm. This technique allowed the correlation of unique points from multiple perspectives within a 3D framework, leading to the creation of a Digital Surface Model (DSM) that captured topographical variations and the intricate geographical elements of the canopy surface [42]. Thus, for each survey area, orthomosaics of each flight were generated for the visible with all bands (Blue, Green and Red), Red Edge (RE) and near-infrared (NIR) bands and the DSM associated. Further insights into these methodologies can be referenced in review works by [43–45] and references within.

2.3. Tree Segmentation

Segmentation in the context of GEOBIA refers to the process by which an image is partitioned into homogeneous regions, called segments or objects. These distinct entities amalgamate pixels sharing analogous attributes like reflectance, texture, and morphology. Contrasting traditional pixel-centric methodologies, OBIA centralizes its analysis on these objectified aggregates, mirroring a more human-centric visual interpretation [46]. For forestry studies, these 'objects' predominantly represent the arboreal tree crowns within the defined area [47].

This study used the multi-resolution algorithm contained in the 'e-Cognition' software (Trimble), which is frequently used in segmentation operations [48,49] and depends on three parameters entered by the user: (1) the homogeneity criteria or scale parameter (ESP), which determines the maximum heterogeneity allowed for the segments generated; (2) the Shape parameter describing the weight of the brightness and shape criteria in the segmentation process; and (3) the Compactness that weight a smoothness criteria to separate the segments [50]. The definition of these parameters for the generation of an optimal segmentation is complex and highly dependent on analysis guided by empirical results [46]. Several exploratory analyses were carried out using different scale parameters and band combinations (e.g. DSM, RE NIR RGB) in conjunction with vegetation indices (e.g. NDVI) as basic inputs for the segmentation tests. Based on these analyses, it was determined that the R,G, B and NIR bands used with parameters of ESP = 120, S= 0.9 and C =0.5 were capable of better discriminating between individual tree segments. It should be noted that these parameters are specific to the particular imaging conditions of this study and are not necessarily reproducible for analysis in other circumstances of resolution and luminosity. A detailed description of the effectiveness of segmentation methods in mangroves can be found in the work by [51].

It is also worth noting that the process of segmenting tree canopy in mangroves is challenging due to their low biodiversity, spectral differentiation between species and overlapping crowns. This characteristic can create undesirable effects such as the suitability of the segmentation parameters, which can well-adjusted the algorithm for one part of the area and worsen the quality of the segmentation in other nearby areas. However, in general, statistically, the set of delineated trees can represent the local structure well, i.e. it is possible to establish, on average, a good estimate of the total number of trees and local concentration, while 'over-segmented' (many segments representing

 doi:10.20944/preprints202408.0539.v1

one tree) or 'under-segmented' (one segment representing several individuals) regions tend to compensate for each other, in which case the objects represent not trees specifically but statistical segments representing the number of individuals in a forest. For a stricter definition, in this case, the objects were called TLO or 'Tree Like Objects' also used in the work of [51].

After segmentation, each TLO was represented as a polygonal feature in a vector file, (e.g. shapefile), stored within a georeferenced database. This allowed for the aggregation of diverse attributes including average intensity values of an object across spectral bands (R, G, B, RE, NIR), and tree height metrics derived from the surface model (e.g., average height, maximum height, height range). Moreover, canopy shape parameters (like area, diameter, shape index, and asymmetry) and texture parameters using the GLCM (Gray-Level Co-occurrence Matrix) method by Haralick were also included. The GLCM captures the spatial relationship between pixel intensities, where the matrix value at (i, j) reveals the frequency of adjacency between pixels of intensities i and j within each TLO. Analysing the GLCM, one can derive texture descriptors. In our study, we focused on the Near Infrared band for its pronounced contrast in vegetative regions and computed GLCM texture parameters including "energy", "entropy", "homogeneity", and "dissimilarity".

In order to better highlight vegetation response, Vegetation Indices were also used to quantify vegetation cover and health by exploiting the differential reflection properties of vegetation across various spectral bands [53–55] The following indices were used: Normalized Difference Vegetation Index (NDVI), Green Vegetation Index (GNVI), Red Edge Vegetation Index (REVI) and Chlorophyll Vegetation Index (CVI).

After completing the calculations for the spectral, textural, shape, and volume features, we structured a Geodatabase using the ArcGIS Pro (3.X) system. This allowed for the creation of thematic maps for each parameter, serving as a foundational layer for the ensuing classification process. Table 1 details the parameters calculated for each Tree Like Object (TLO) along with their descriptions.

Table 1. Spectral, textural and shape features extracted from the trees segments.

TREE OBJECT FEATURES	DESCRIPTION
REFLECTANCE	
DJI 1 - Blue	Band reflectance at 450 nm ± 16 nm
DJI 2 - Green	Band reflectance at 560 nm ± 16 nm
DJI 3 - Red	Band reflectance at 650 nm ± 16 nm,
DJI 4 – Red Edge	Band reflectance at 730 nm ± 16 nm
DJI 5 – Near Infra Red	Band reflectance at 840 nm ± 26 nm
Brightness	Total albedo in all bands
Brightness variance	(max – min albedo in all bands)
NDVI (Mean)	$\frac{\mathrm{NIR}-\mathrm{Red}}{\mathrm{NIR}+\mathrm{Red}}$
GNVI (Mean)	$\frac{\mathrm{Green}-\mathrm{NIR}}{\mathrm{Green}+\mathrm{NIR}}$
CVI (Mean)	$\frac{NIR-RE}{NIR+RE}$
REVI (Mean)	$\mathrm{NIR}*\frac{\mathrm{Red}}{\mathrm{Green}^2}$
DIGITAL SURFACE MODEL	
Tree Hight (Mean)	Mean value of DSM pixels within the polygon
Tree Hight (Maximum)	Maximum value of DSM pixels within the polygon
SHAPE	
Demeter	Diameter of Tree polygon
Area	Area of Tree polygon

 doi:10.20944/preprints202408.0539.v1

Shape Index*	$\frac{b_v}{4\sqrt{\#P_v}}$	b_v= object border length $4\sqrt{\#P_v}$ = border of a square with area #Pv
Roundness*	$\varepsilon_v^{\max} - \varepsilon_v^{\min}$	$\varepsilon_v^{\max}$ = radius of the smallest enclosing ellipse $\varepsilon_v^{\min}$ = radius of the largest enclosed ellipse
Assimetry*	$\frac{2\sqrt{\frac{1}{4}(\mathrm{Var}X + \mathrm{Var}Y)^2 + (\mathrm{Var}XY)^2 - \mathrm{Var}X \cdot \mathrm{Var}Y}}{\mathrm{Var}X + \mathrm{Var}Y}$	$VarX$ = variance of X $VarY$= variance of Y
Border Index*	$\frac{b_v}{2\,(l_v + w_v)}$	b_v = Tree Object border length l_v = length of the tree object w_v = width of the tree object
Mean Direction*	$\frac{180^\circ}{\pi}\tan^{-1}(\mathrm{Var}XY, \lambda_1 - \mathrm{Var}Y) + 90^\circ$	$VarX$ = variance of X $VarY$= variance of Y λ_1 = eigenvalue
TEXTURE (GLCM)		
Entropy*	$\sum_{i,j=0}^{N-1} P_{i,j}\,(-\ln P_{i,j})$	i = GLCM row number j = GLCM column number $P_{i,j}$ = the normalized value in the cell i;j N = number of rows or columns $\mu_{i,j}$ = the GLCM mean $\sigma_{i,j}$ = the GLCM standard deviation
Dissimilarity*	$\sum_{k=0}^{N-1} k\,(V_k)$	
Energy*	$\sum_{i,j=0}^{N-1} (P_{i,j})^2$	
Homogenity*	$\sum_{i,j=0}^{N-1} \frac{P_{i,j}}{1 + (i-j)^2}$	

2.4. Field Data

To correlate the data obtained by UAVs with direct in situ measurements, five forest inventory plots were established, two in the Suape area and three in the Cardoso Island area (see figure 1 and 2 for geographic reference).

The structure attributes of the mangrove vegetation were obtained in delimited plots of variable size using the methodology proposed by Schaeffer-Novelli [56]. Diameter at breast height (DBH) measurements were taken from plants over 1m in height. Georeferenced species identification and determination of the number of live and dead trunks were carried out. The areas of the plots were determined to contain at least 20 individuals over 2m in height each. The areas of the plots were chosen to cover the mangrove sub-environments such as the fringe and basin to obtain data representative of the structure of the forest.

The highest trees were individually photographed measured and geo-referenced and correlated with the canopies identified on the identification (50m) and mapping (120m) UAV flights and then used as training samples for the classification process (see item 2.5). The heights and diameters of the canopies were also measured using laser rangefinders to calibrate the digital elevation models and segmentation algorithms.

2.5. Classification

Classification in remote sensing and geospatial analysis involves categorizing objects based on attributes like spectral signatures, texture, and spatial context [46,57]. The classification focused on

 doi:10.20944/preprints202408.0539.v1

the taxonomic identification of the mangrove, i.e., it sought to identify the species of the trees delimited by the segmentation process for each object based on known training samples identified in the forest plots and UAV detail flights (i.e. supervised classification [58]). Although mangroves have a low biodiversity, their classification can be a challenge since different tree species can have similar spectral, textural and shape characteristics and, on the other hand, within a single species, there can be significant variations in terms of shape, size and spectral appearance, depending on local growing conditions (see details in [59,60,61,62].

In this regard, Machine Learning (ML) algorithms have proven particularly useful, as they offer a great capacity to model non-linear relationships and complex interactions between variables based on training samples, which may not be captured by more traditional methods. This capability is especially valuable in environments where spectral, textural, and contextual features interrelate in intricate ways, particularly as in the case of mangroves [63]. Among the most notable ML techniques, deep learning, such as Deep Neural Networks (DNNs), stands out for its ability to learn features directly from the data, avoiding the need for meticulous manual feature engineering [64]. Ensemble models, such as Random Forest and Naive Bayes, combine multiple models or decision trees for more robust classification and to minimize the risk of overfitting the training data. A full review of the details of each of the main ML algorithms and details on the formalism and parameterization of the models is detailed in [65,66].

The following classes was considered Rhizophora mangle, L. racemosa and A. schauerianna, however for the Suape region the species A. schauerianna was not considered since its occurrence in the mangrove is significantly rarer (corroborated by the literature like and the forest inventory plot data which did not identify any occurrence of this species). The 'gap/shadows' class was also considered for objects with low reflectance, as well as the 'channel/water' and 'sandbank' classes in non-vegetated areas. In the Suape region, the "Other" class was also considered, since regions of coastal vegetation (different from mangroves) were identified in some areas, specifically on the borders of the study area.

Training samples for the classifiers were sourced from images captured during low-altitude flights (with a resolution of 30m to 1.4cm per pixel). These images were specifically linked to trees that were measured on-site in areas where the canopy of the species was identified in the field. For each class, a minimum of 130 samples were designated, with 100 allocated for training purposes and the remaining used to test the models' accuracy.

The modelling was developed using a script in 'Python' (via the 'NumPy and 'Sklearn' libraries) and reproduced in the 'Orange Data Mining 3.2.' software for the preparation of graphs and statistical tests. After various model parameterization tests, the best results (e.g. models that best 'fit' the data distribution) were incorporated into the previously described OBIA data models.

2.7. Analyzing Species Spatial Distribution

Once species have been classified based on segmentation and classification supported by tying in with field measurements, a logical next step for a high-resolution analysis is to assess the spatial distribution of these trees, specifically with regard to the ordering (e.g. concentration and/or random distribution) of the species in the mangrove ecosystem. Various metrics can be used to determine this spatial patterning and it is not the focus of this study to evaluate each of them. A vast biography can be found in works such as [67,68]. One of the most direct forms for this type of analysis is the determination of hot spot zones for each species using Gi* (Getis-Ord) spatial statistics. This method identifies clusters of high values (hot spots) and low values (cold spots) within the study area, providing a clear visualization of the spatial intensity and distribution patterns of different species.

Each species in the two studied areas was summarized within a grid (fishnet) with 20m resolution where Gi* Score statistic was calculated to assess the degree of spatial clustering, with positive Gi* Scores indicating hot spots and negative scores indicating cold spots. P-values associated with each Gi* Score were computed to determine the statistical significance of the observed clustering, identifying cells with statistically significant Gi* Scores as true hot spots or cold spots. The results were displayed using as maps, highlighting areas of significant species concentration and

 doi:10.20944/preprints202408.0539.v1

dispersion. Detailed methods of Getis-Ord spatial statistics applied to forest application can be accessed in [69,70].

Figure 3 presents the study's conceptual and methodological scheme, succinctly outlining the research framework and analytical steps employed in this article.

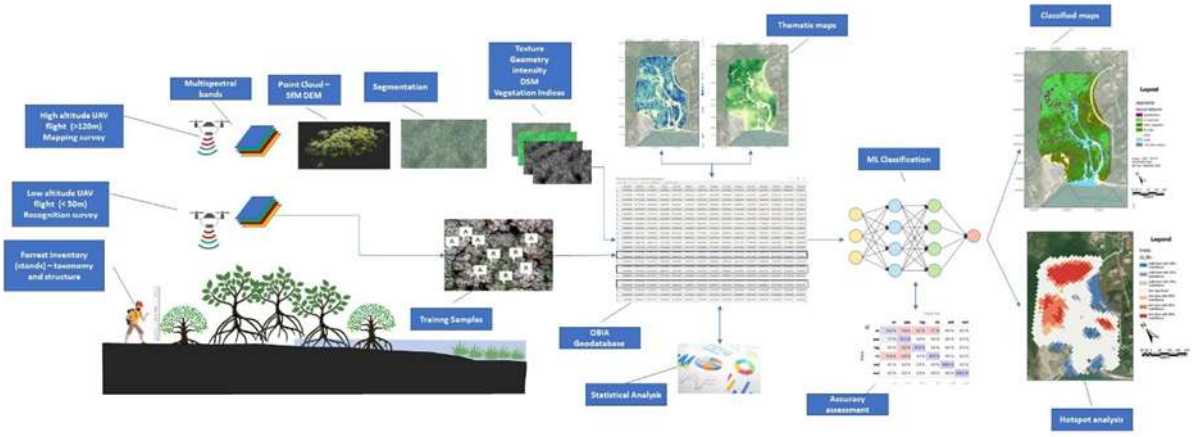

Figure 3. - Conceptual and methodological scheme of the work.

3. Results

The use of OBIA (Object-Based Image Analysis) has proven effective for classifying mangroves using high-resolution UAV (Unmanned Aerial Vehicle) imaging. This approach relies on two main processes: segmentation and subsequent classification. Segmentation of trees and mangrove forests, however, is complex and challenging to apply universally. Segmentation parameters, such as edge index and scale, often work well for one region of the study area but not for others. For instance, parameters that fit the Cardoso Island region did not apply to the Suape region, necessitating empirical adjustments for each area. Nevertheless, by using field-obtained data from the tops of the plots, it was possible to fine-tune the parameters to the local context and then generalize them to other study regions. The use of infra-red and red-edge bands has significantly enhanced crown discrimination, reducing the subjectivity of applying segmentation parameters compared to using RGB images alone.

Through the segmentation process, tree crowns could be individualized. By extracting values related to their shape, texture, and spectral indices, a series of parameters could be associated with these objects (or Tree-Like Objects, TLOs). This resulted in the creation of a structured database within the ESRI ArcGIS Pro platform. This database comprises the 24 distinct parameters, organized as detailed in Table 1 (section 2.3). This enabled the creation of thematic maps for all stored parameters, facilitating the development of vegetation structure atlases. Such atlases could include data on average tree height, crown area, diverse vegetation indices, and both geometric and textural parameters. These comprehensive map collections are crucial for conducting broad analyses of mangrove vegetation's structural patterns, offering insights into generic aspects of vegetation like biomass estimates, which can readily be acquired from UAV flights conducted at mapping altitudes surveys, straightforward and cost-effective.

Figure 4 and 5 show examples of thematic maps for the Cardoso Island and Suape regions, respectively, highlighting distributions of geometric variables (shape index), texture (represented by entropy), the average DSM value which indicates tree height, and the NDVI reflecting vegetation vigour and coverageThis section may be divided by subheadings. It should provide a concise and precse description of the experimental results, their interpretation, as well as the experimental conclusions that can be drawn.

 doi:10.20944/preprints202408.0539.v1

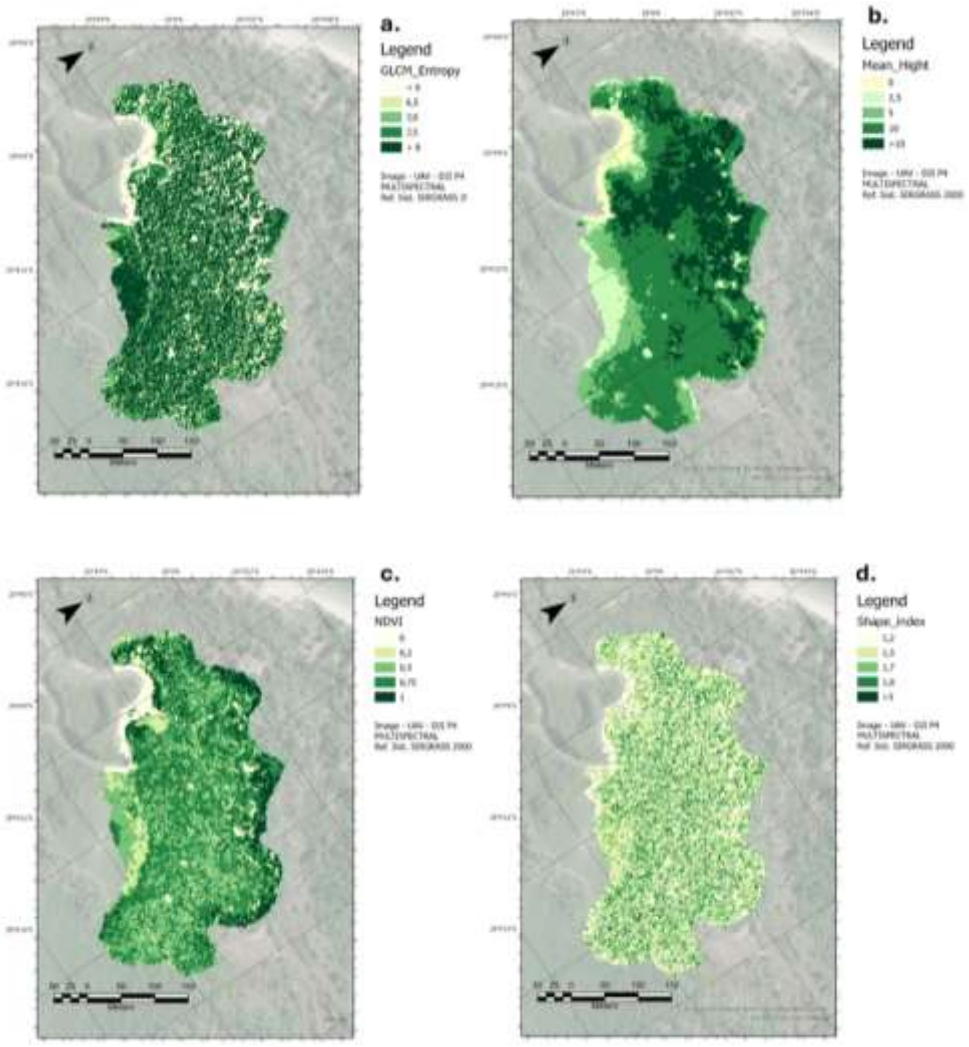

Figure 4. – Thematic maps of tree parameters of Cardoso Island (SP) Mangrove. a) GLCM Entropy, b) Tree mean High, c) NDVI d) Shape Index.

 doi:10.20944/preprints202408.0539.v1

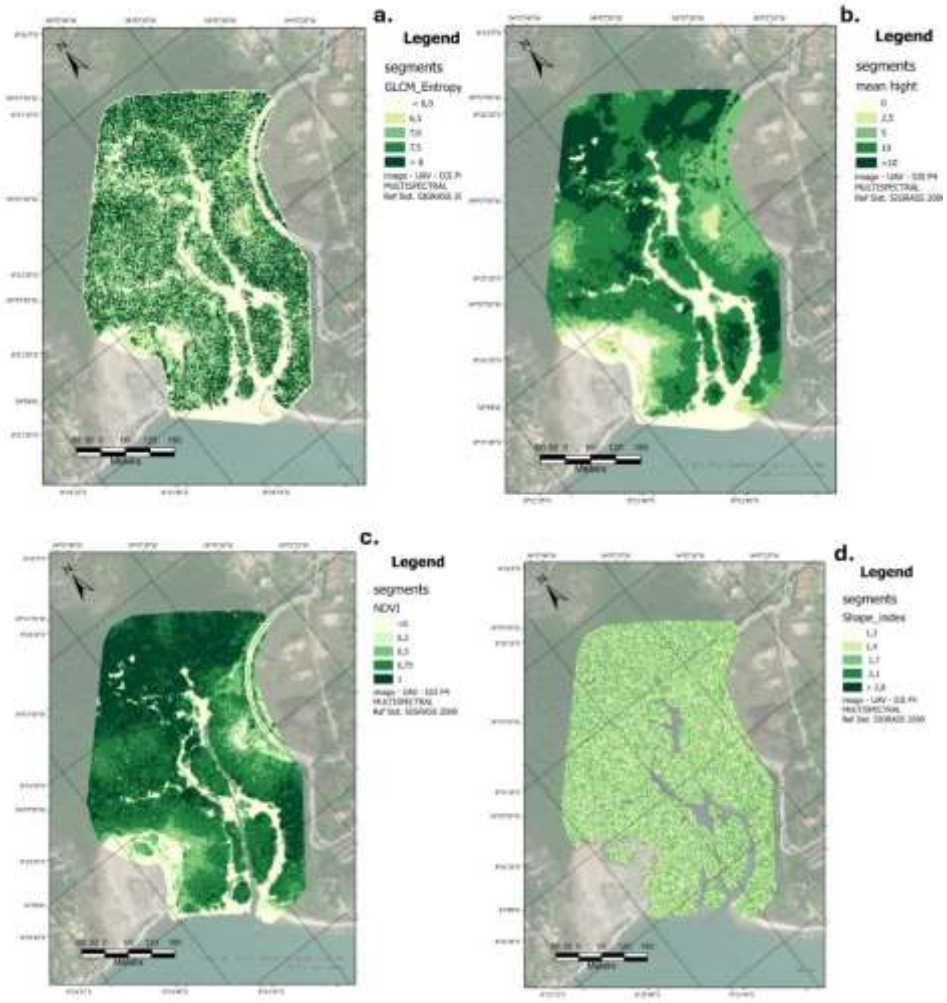

Figure 5. – Thematic maps of tree parameters of Suape (PE) Mangrove. a) GLCM Entropy, b) Tree mean High Height, c) NDVI d) Shape Index.

Based on this information, three supervised classification algorithms based on Machine Learning (ML) were applied to classify the study areas: "Random Forest", "Naive Bayes" and "Deep Neural Network". The figures 6 and 7 show in the form of confusion matrices the capacity of each of the algorithms used to discriminate each of the classes for Cardoso Island and Suape respectively. Based on these models, species classification maps were generated for the areas (represented in the maps shown in figures 8 for Cardoso Island region and 9 for the Suape region). After various model parameterization tests, the best results (e.g. models that best 'fit' the data distribution) were incorporated into the previously described OBIA data models.

 doi:10.20944/preprints202408.0539.v1

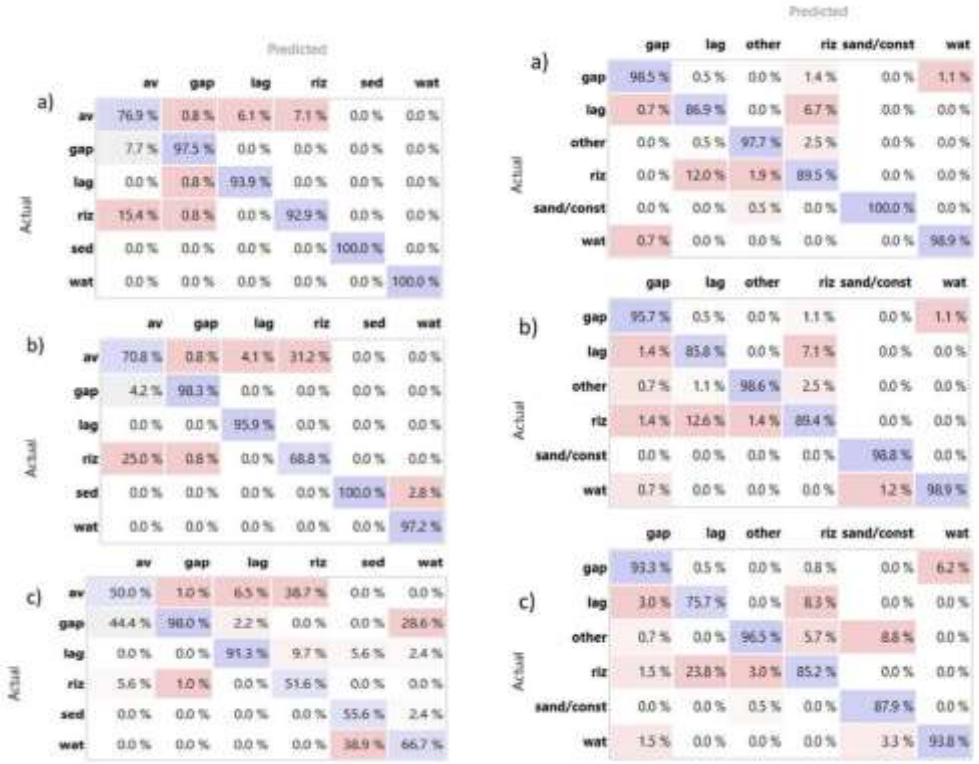

Figure 6. - Confusion matrix for classifying TLOs in the Cardoso Island region using the 'random Forrest' (a) and Naive Bayes (b) Neural Network (c) algorithms.

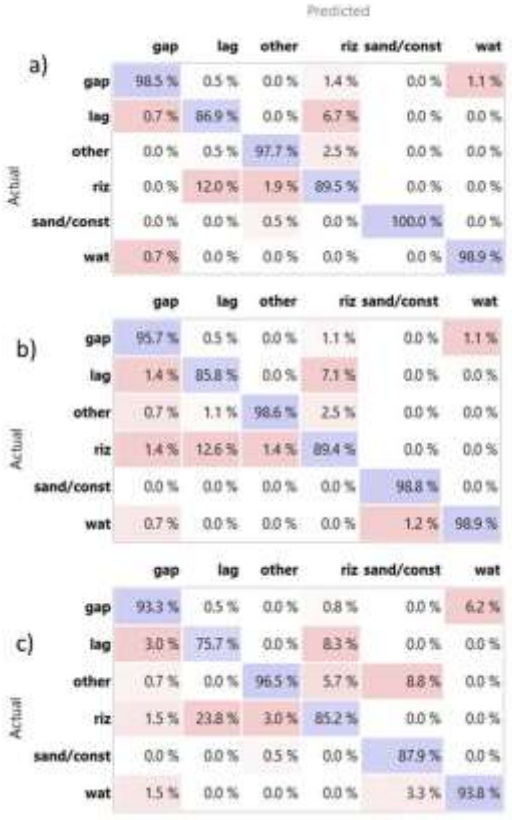

Figure 7. - Confusion matrix for classifying TLOs in the Suape region using the 'random Forest' (a) and Naive Bayes (b) Neural Network (c) algorithms.

 doi:10.20944/preprints202408.0539.v1

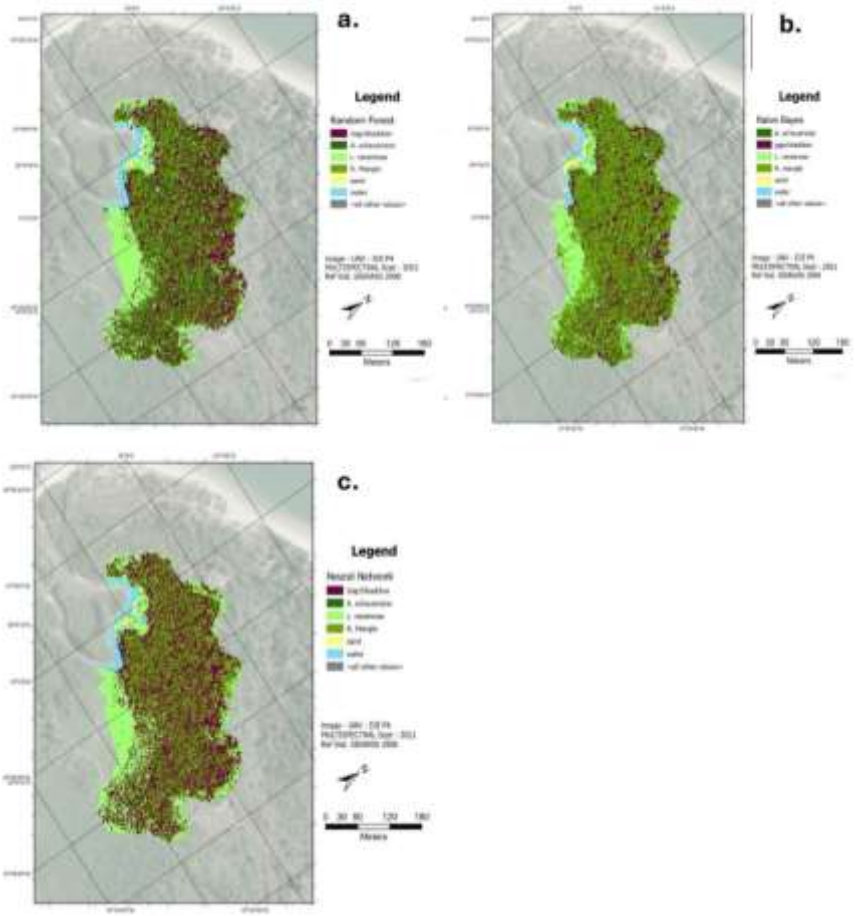

Figure 8. - TLO classification maps for the Cardoso Island region based on the random Forest (a) and Naive Bayes (b) Neural Network (c) algorithms.

 doi:10.20944/preprints202408.0539.v1

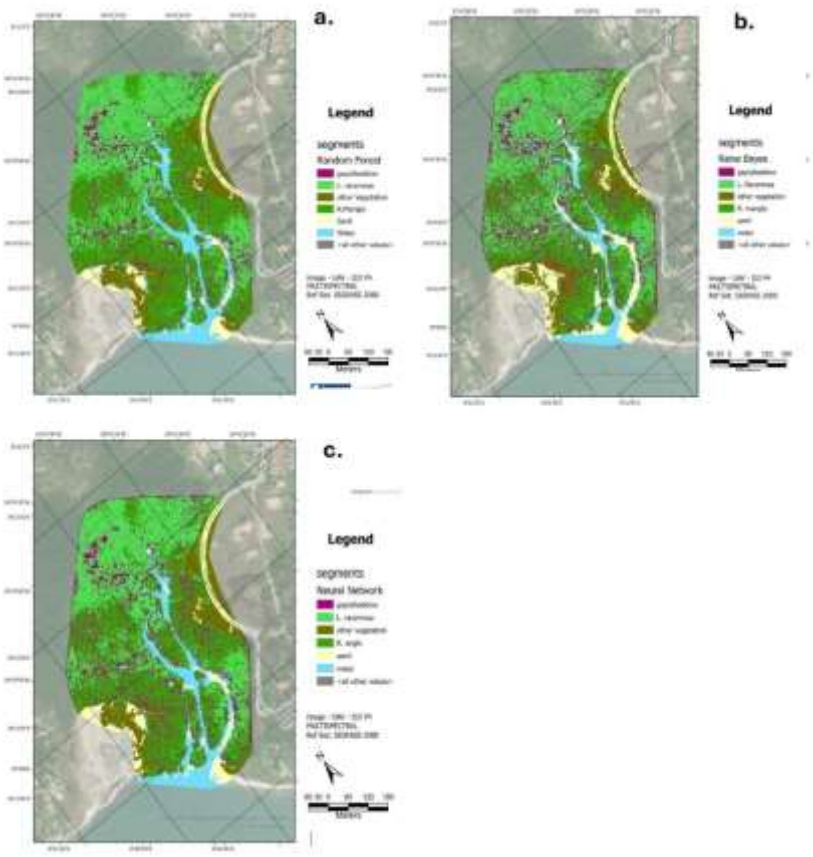

Figure 9. TLO classification maps for the Suape region based on the random Forest (a) and Naive Bayes (b) Neural Network (c) algorithms.

In the two studies sites, the Random Forest models showed slightly better accuracy. This was particularly evident for Cardoso Island, where the classifiers struggled more with the presence of R. mangle and A. schaeriana specimens. However, all algorithms were better at differentiating L. racemose trees in both the Cardoso Island and Suape regions. Consequently, the distribution based on the Random Forest model was used for subsequent analyses as reference.

The distribution of tree species exhibited a distinct zonation in the two study areas. Hotspot analyses based on the Gi*-ord statistic revealed a clear compartmentalization in Cardoso Island (Figure 10). In this area, L. racemosa predominates in the fringe regions, particularly near the estuarine channel (Figure 10 b), while R. mangle and A. schaueriana are concentrated in the inner portions of the mangrove, sharing the same area (Figures 10a). In contrast, the Suape Mangrove presents a different pattern. Despite the absence of A. schaueriana, L. racemosa primarily concentrates in the inner portions of the mangrove, whereas R. mangle is found in the areas closest to the estuarine channel. (figure 10 c and d)

 doi:10.20944/preprints202408.0539.v1

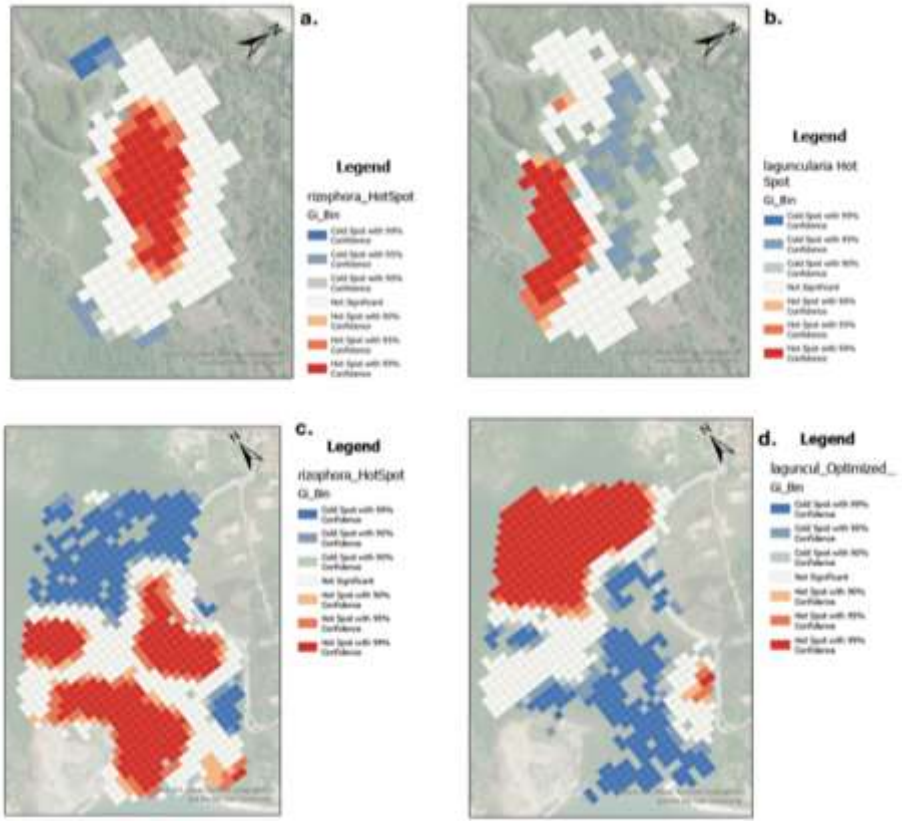

Figure 10. – HotSpot distribution maps of main arboreal species: Rizophora Mangle and b. Laguncularia Racemosa in Cardoso Island and c. Rizophora Mangle and d. Laguncularia Racemosa in Suape Region.

The two regions exhibited differences not only in tree species distribution but also in structural characteristics. For instance, considering only R. mangle trees, those in the Suape region generally had larger canopy areas, averaging 7.2 m². Conversely, trees in the Cardoso Island mangrove had a smaller average canopy area of 4.95 m². Interestingly, average heights displayed a reverse trend: R. mangle trees in Suape averaged a height of 6.5 m, while those in the Cardoso Island mangrove stood taller, with an average height of 8.8 m, as shown in the tree distribution histograms in Figure 11. On the other hand, L. racemosa trees had a significantly higher average height in Suape (8,5m) compared to Cardoso Island (4,2m).

 doi:10.20944/preprints202408.0539.v1

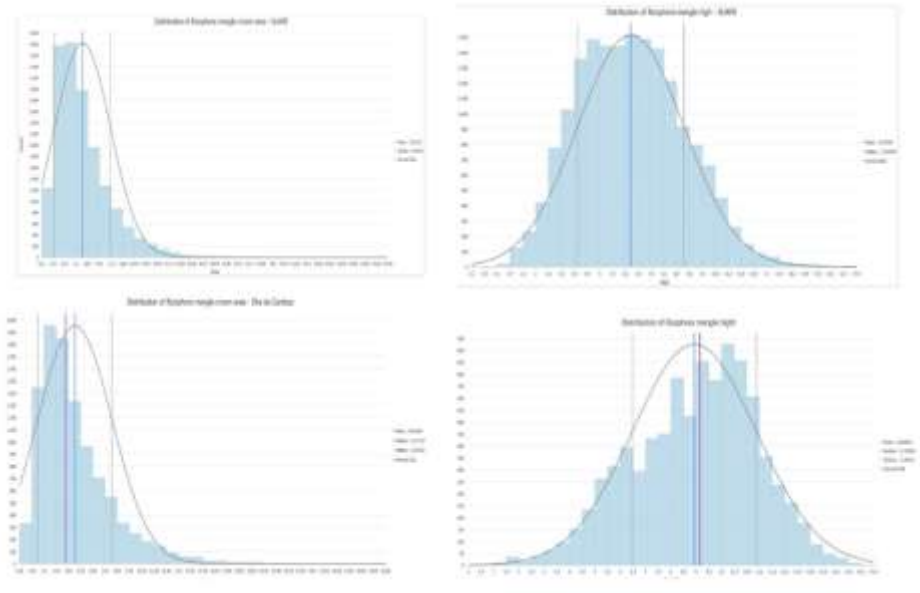

Figure 11. Histograms of the distribution of canopy heights and areas (TLOs) specifically of the *R. mangle* trees for the Suape region (a and b) and Cardoso Island (c and d).

The establishment of a geodatabase of specific trees, or Tree-Like Objects (TLOs), with multiple associated parameters opens up a myriad of possibilities for data representation. Among these, the creation of 3D models stands out, as the height of the trees can be estimated using Digital Surface Models (DSM). In these 3D representations, each species is symbolized by a rendered icon with a height proportional to the actual tree, providing an intuitive and detailed visual representation. This approach is incredibly useful for visualization and decision-making processes, offering stakeholders a clear, interactive way to understand spatial patterns and the characteristics of different tree species. Figure 12 illustrates examples of synthetic 3D visualizations of mangroves, showcasing data linked to specifically chosen trees, thereby highlighting the utility of this method in environmental analysis and management

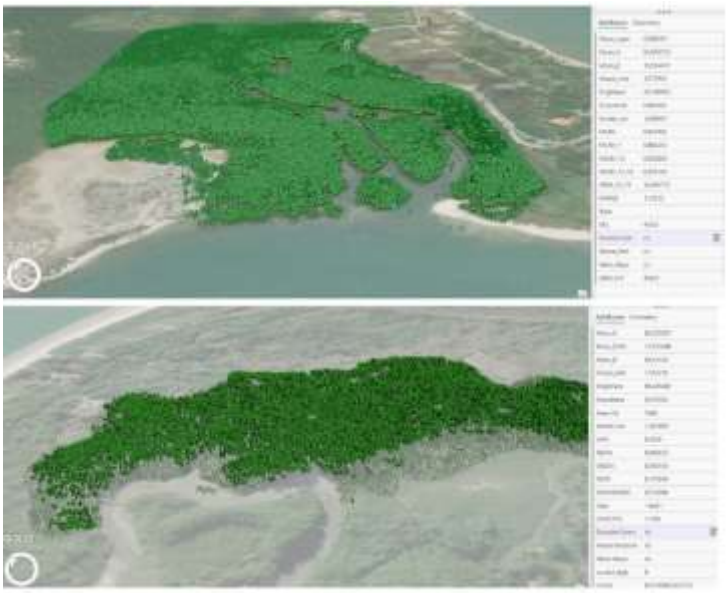

Figure 12. – 3D representation of mangroves – each tree represents the proportional tree highs in Suape (upper) and Cardoso Island (lower). The selected object (TLO) allows the visualization of all parameters described in table 1.

 doi:10.20944/preprints202408.0539.v1

4. Discussion

The method used for mapping mangroves from multispectral UAV imagery using object-based image analysis (OBIA) proved to be effective to segment and classify tree species in mangrove forests, in particular in the selected studied areas. Multispectral images have demonstrated clear superiority over conventional RGB images, particularly in the processes of segmenting tree canopies and in classification tasks. These additional spectral bands provided critical information that improved the distinction between different vegetation types and health conditions, thereby leading higher accuracy. The use of texture parameters (GLCM) and band ratios (derived from vegetation indices) proved quite important in enhancing the classification process. In contrast, the shape indices had minimal impact on the performance of the classifiers algorithms.

Using two survey altitudes, specifically 120 meters and 50 meters, further optimized the mapping process. Higher altitude flights, referred to as 'mapping resolution,' allowed for the coverage of larger areas, which is essential for comprehensive landscape-level mapping. In the other hand, lower altitude flights, or 'detail resolution,' facilitated the identification of species within smaller survey areas due to the finer resolution of the images captured. This approach, combined with in situ validation plots, was crucial for training the classification models in a more efficient and accurate manner. The dual-altitude strategy ensured that both broad-scale and fine-scale details were effectively captured and analysed, resulting in a robust and thorough mapping of mangrove ecosystems.

Regarding the object classifier performance, the Random Forest model exhibited slightly better performance compared to Deep Neural Networks and Naive Bayes due to its ensemble learning approach, which combines multiple decision trees to enhance predictive accuracy. Unlike Deep Neural Networks, which require extensive training data, Random Forests efficiently handle smaller datasets and are less prone to overfitting such as the case of this study. Additionally, the simplicity of Random Forests in dealing with feature interactions and non-linear relationships gave them an edge over the more complex Deep Neural Networks and the simpler, probabilistic-based Naive Bayes. This balance of complexity and interpretability made Random Forests particularly effective in differentiating between species in ecological datasets, where the presence of certain specimens, such as R. mangle and A. schaeriana, introduced variability and classification challenges. These results corroborate other similar studies of mangrove species classification using UAVs, specifically the work by [18].

A clear difference in the zonation of the two studied mangroves was observed, despite having the same species. In Suape, an estuary with larger tidal amplitudes, low freshwater input, and terrigenous material, the mangrove swamp is sandier hence the trees are more densely established with fewer gaps, with predominance of Rhizophora mangles with more laterally extensive roots, resulting in trees with larger canopies. In contrast, the Cardoso Island region, characterized by less intense tides and higher input of muddy material (also associated with greater rainfall and freshwater in the estuarine system), features a mangrove with a muddier texture, taller trees, and more gaps, likely due to local tree falls and a less firm substrate. Additionally, small concentrations of L. racemosa are found in fringe areas of the Cardoso Island mangrove, where coarser sediments have been deposited, indicating this species is associated to coarser texture substrate. In Suape, L. racemosa specimens are significantly taller, with sizes comparable to those of R. Mangle, the relationship of the size and distribution of mangrove trees and their relationships with the sediment texture and tidal flows was described in [71–74].

An important point is that once the most significant parameters for classification have been established and an automatic classification routine has been set up, it becomes possible to create an automated practice for mapping mangrove areas, allowing for significant savings in time and resources. It should also be emphasised that the repeatability of this method in different areas could also allow a training image library to be developed (e.g. from detail flights), improving supervised classification algorithms.

More in-depth analyses of distribution and spatial correlations can lead to more complex conclusions about the distribution of species in mangrove ecosystems and their relationships with

 doi:10.20944/preprints202408.0539.v1

external factors. For example, niche analyses that are normally carried out on a regional scale can be developed at the level of small areas. In addition, the estimation of biophysical parameters, such as biomass, through the application of species-specific allometric equations can significantly improve the accuracy of Blue Carbon estimations furthermore it can be important to calibrate regional or global blue carbon inventories. However, sub-stratum vegetation is not imaged, which may introduce significant uncertainty into these estimates.

5. Conclusions

The study demonstrates the significant potential of UAV technology for high-resolution mapping of mangrove ecosystems. UAV-based multispectral imagery combined with Object-Based Image Analysis (OBIA) has proven effective in accurately segmenting and classifying mangrove tree species, providing detailed spatial distributions that are crucial for ecological analysis. This approach enhances the understanding of species-specific patterns and health conditions within mangrove forests. Multispectral imagery, with its additional spectral bands, significantly improves species classification accuracy compared to conventional RGB images. These bands provide critical information for distinguishing between different vegetation types and health conditions, essential for precise ecological assessments. The study's examples of the two mangroves illustrate the zonal complexity within small areas, explained by their differing geological and hydrodynamic settings. Despite these advancements, several challenges remain. Developing universal parameters for segmentation and classification across different mangrove ecosystems is desirable but not yet feasible. Additionally, UAV technology's focus on the upper canopy neglects the lower forest strata, potentially limiting the understanding of complete ecological processes within the mangrove forest. Addressing these challenges in future studies will enhance the comprehensiveness and accuracy of UAV-based mangrove mapping, contributing to more effective conservation and management of these ecosystems.

6. Acknowledgements

We thank Prof. Teodoro Isnard de Almeida and Prof. Alexander Turra from the University of São Paulo, as well as Edson Rodrigues do Nascimento, for their invaluable expertise and guidance. Special thanks to the administration and staff of the Cardoso Island State Park (Fundação Florestal - São Paulo) for their field support. This research was funded by the São Paulo Research Foundation (Fundação de Amparo à Pesquisa do Estado de São Paulo - FAPESP), processes 2019/22821-0 and 2023/10107-9.

References

1. Schwenke, T., & Helfer, V. (2021). Beyond borders: The status of interdisciplinary mangrove research in the face of global and local threats. Estuarine, Coastal and Shelf Science, 250, 107119.
2. Ewel, K., Twilley, R., & Ong, J. I. N. (1998). Different kinds of mangrove forests provide different goods and services. Global Ecology & Biogeography Letters, 7(1), 83-94.
3. Vo, Q. T., Künzer, C., Vo, Q. M., Moder, F., & Oppelt, N. (2012). Review of valuation methods for mangrove ecosystem services. Ecological indicators, 23, 431-446.
4. Cunha-Lignon, M., Mendonça, J. T., Conti, L. A., de Souza Barros, K. V., & Magalhães, K. M. (2023). Mangroves and Seagrasses. In Blue Economy: An Ocean Science Perspective (pp. 55-85). Singapore: Springer Nature Singapore.
5. Windle, A. E., & Silsbe, G. M. (2021). Evaluation of unoccupied aircraft system (UAS) remote sensing reflectance retrievals for water quality monitoring in coastal waters. Frontiers in Environmental Science, 9, 674247
6. Walker, J. E., Ankersen, T., Barchiesi, S., Meyer, C. K., Altieri, A. H., Osborne, T. Z., & Angelini, C. (2022). Governance and the mangrove commons: Advancing the cross-scale, nested framework for the global conservation and wise use of mangroves. Journal of environmental management, 312, 114823.
7. Adade, R., Aibinu, A. M., Ekumah, B., & Asaana, J. (2021). Unmanned Aerial Vehicle (UAV) applications in coastal zone management—A review. Environmental Monitoring and Assessment, 193, 1-12.
8. Singhal, G., Bansod, B., & Mathew, L. (2018). Unmanned aerial vehicle classification, applications and challenges: A review.

9. Lorah, P., Ready, A., & Rinn, E. (2018). Using drones to generate new data for conservation insights. International Journal of Geospatial and Environmental Research, 5(2), 2.
10. Ruwaimana, M., Satyanarayana, B., Otero, V., M. Muslim, A., Syafiq A, M., Ibrahim, S., ... & Dahdouh-Guebas, F. (2018). The advantages of using drones over space-borne imagery in the mapping of mangrove forests. PloS one, 13(7), e0200288.
11. Yaney-Keller, A., Santidrián Tomillo, P., Marshall, J. M., & Paladino, F. V. (2019). Using Unmanned Aerial Systems (UAS) to assay mangrove estuaries on the Pacific coast of Costa Rica. PLoS One, 14(6), e0217310.
12. Castellanos-Galindo, G. A., Casella, E., Mejía-Rentería, J. C., & Rovere, A. (2019). Habitat mapping of remote coasts: Evaluating the usefulness of lightweight unmanned aerial vehicles for conservation and monitoring. Biological Conservation, 239, 108282.
13. Hsu, A. J., Kumagai, J., Favoretto, F., Dorian, J., Guerrero Martinez, B., & Aburto-Oropeza, O. (2020). Driven by drones: Improving mangrove extent maps using high-resolution remote sensing. Remote Sensing, 12(23), 3986.
14. Kabiri, K. (2020). Mapping coastal ecosystems and features using a low-cost standard drone: Case study, Nayband Bay, Persian gulf, Iran. Journal of Coastal Conservation, 24(5), 62.
15. Salim, H. L., Adi, N. S., Kepel, T. L., & Ati, R. N. A. (2020, August). Estimating mangrove biomass using drone in Karimunjawa Islands. In IOP Conference Series: Earth and Environmental Science (Vol. 561, No. 1, p. 012054). IOP Publishing.
16. Arfan, A., Nyompa, S., Maru, R., Nurdin, S., & Juanda, M. F. (2021, November). Mapping analysis of mangrove areas using Unmanned Aerial Vehicle (UAV) method in Maros District South Sulawesi. In Journal of Physics: Conference Series (Vol. 2123, No. 1, p. 012010). IOP Publishing.
17. Thoha, A. S., Lubis, O. A., Hulu, D. L. N., Sari, T. Y., Ulfa, M., & Mardiyadi, Z. (2022). Utilization of UAV (Unmanned Aerial Vehicle) technology for mangrove species identification in Belawan, Medan City, North Sumatera, Indonesia. In IOP Conference Series: Earth and Environmental Science (Vol. 1115, No. 1, p. 012074). IOP Publishing.
18. Miraki, M., Sohrabi, H., Fatehi, P. and Kneubuehler, M., 2021. Individual tree crown delineation from high-resolution UAV images in broadleaf forest. Ecological Informatics, 61, p.101207.
19. Nellemann, C., Corcoran, E., Duarte, C.M., Valdez, L., DeYoung, C., Fonseca, I., Grimsditch, G., 2009. Blue Carbon. A Rapid Response Assessment. United Nations Enviroment Programme.
20. Lovelock, C. E., & Duarte, C. M. (2019). Dimensions of blue carbon and emerging perspectives. Biology letters, 15(3), 20180781.
21. Zeng, Y., Friess, D. A., Sarira, T. V., Siman, K., & Koh, L. P. (2021). Global potential and limits of mangrove blue carbon for climate change mitigation. Current Biology, 31(8), 1737-1743.
22. Jones, A. R., Raja Segaran, R., Clarke, K. D., Waycott, M., Goh, W. S., & Gillanders, B. M. (2020). Estimating mangrove tree biomass and carbon content: a comparison of forest inventory techniques and drone imagery. Frontiers in Marine Science, 6, 784.
23. Zimudzi, E., Sanders, I., Rollings, N., & Omlin, C. W. (2021). Remote sensing of mangroves using unmanned aerial vehicles: Current state and future directions. Journal of Spatial Science, 66(2), 195-212.
24. Basyuni, M., Wirasatriya, A., Iryanthony, S. B., Amelia, R., Slamet, B., Sulistiyono, N., ... & Arifanti, V. B. (2023). Aboveground biomass and carbon stock estimation using UAV photogrammetry in Indonesian mangroves and other competing land uses. Ecological Informatics, 77, 102227.,
25. Ngo, D., Nguyen, H., Nguyen, K., Dang, C., Nguyen, H., Dang, N., & Pham, T. (2023). Application of multispectral UAV to estimate mangrove biomass in Vietnam: A case study in Dong Rui commune, Quang Ninh Province. One Ecosystem, 8, e103760.
26. Chen, G., Weng, Q., Hay, G. J., & He, Y. (2018). Geographic object-based image analysis (GEOBIA): Emerging trends and future opportunities. GIScience & Remote Sensing, 55(2), 159-182.
27. Li, Y., Fu, B., Sun, X., Fan, D., Wang, Y., He, H., ... & Yao, Y. (2022). Comparison of Different Transfer Learning Methods for Classification of Mangrove Communities Using MCCUNet and UAV Multispectral Images. Remote Sensing, 14(21), 5533.
28. Fernandez, G. B., da Rocha, T. B., Barboza, E. G., Dillenburg, S. R., da Camara Rosa, M. L. C., Angulo, R. J., ... & Dominguez, J. M. L. (2019). Natural landscapes along Brazilian coastline. The Physical Geography of Brazil: Environment, Vegetation and Landscape, 199-218.
29. Conti, L. A., Araujo, C. A. S., Paolo, F. S., Barcellos, R. L., Rodrigues, M., Mahiques, M. M., & Furtado, V. V. (2012). An integrated GIS for sedimentological and geomorphological analysis of a lagoon environment. Barra de Cananéia inlet region (Southeastern Brazil). Journal of coastal conservation, 16, 13-24.
30. Cunha-Lignon, M., Kampel, M., Menghini, R. P., Schaeffer-Novelli, Y., Cintrón, G., & Dahdouh-Guebas, F. (2011). Mangrove forests submitted to depositional processes and salinity variation investigated using satellite images and vegetation structure surveys. Journal of coastal research, 344-348.
31. Schaeffer-Novelli, Y., Cintrón-Molero, G., Adaime, R. R., & de Camargo, T. M. (1990). Variability of mangrove ecosystems along the Brazilian coast. Estuaries, 13, 204-218.

32. Schröter, B.; Sessin-Dilascio, K.; Meyer, C.; Matzdorf, B.; Sattler, C.; Meyer, A.; Giersch, G.; Jericó-Daminello, C.; Wortmann, L. Multi-level governance through adaptive co management: conflict resolution in a Brazilian state park. Ecological Processes, v. 3, n. 1, 2014. https://doi.org/10.1186/2192-1709-3-6
33. Cunha-Lignon, M., Coelho Jr, C., Almeida, R. D., Menghini, R., Correa, F., Schaeffer-Novelli, Y., ... & Dahdouh-Guebas, F. (2009). Mangrove forests and sedimentary processes on the South of Coast of São Paulo State (Brazil). Journal of Coastal Research, 405-409.
34. Oliveira, T.S., Xavier, D. de A., Santos, L.D., França, E.J., Sanders, C.J., Passos, T.U., Barcellos, R.L., 2020. Geochemical background indicators within a tropical estuarine system influenced by a port-industrial complex. Mar. Pollut. Bull. 161, 111794
35. Oliveira, T. S., Xavier, D. D. A., Santos, L. D., Passos, T. U., Sanders, C. J., França, E. J., Camargo, P. B., Penny D. & Barcellos, R. L. (2021). Reconstructing the history of environmental impact in a tropical mangrove ecosystem: A case study from the Suape port-industrial complex, Brazil. Regional Studies in Marine Science, 44, 101747.
36. Fernandes, L.M.B., 2000. Avaliação dos ambientes recifais do litoral de Pernambuco, através das suas macro e megafaunas incrustantes e sedentárias (Doctoral Thesis). Universidade de São Paulo, IOUSP.
37. Barcellos, R.L., Santos, L.D. dos, 2018. Histórico de impactos ambientais e o estado da arte em Oceanografia no sistema estuarino-lagunar de Suape-Ipojuca (PE). Parcer. Estratégicas 23, 155–168.
38. Zanardi-Lamardo, E., Schettini, C. A. F., Vieira-Campos, A. A., Cabral, C. B., & Silva, M. S. (2018). Intratidal variability and transport of petroleum aromatic hydrocarbons in an anthropized tropical estuarine system: the Suape estuary (8.4 S 35W). Brazilian Journal of Oceanography, 66, 47-57.
39. Passos, T., Penny, D., Sanders, C., De França, E., Oliveira, T., Santos, L., Barcellos, R., 2021. Mangrove carbon and nutrient accumulation shifts driven by rapid development in a tropical estuarine system, northeast Brazil. Mar. Pollut. Bull. 166, 112219.
40. Braga, R. A. P., Uchoa, T. M. D. M., & Duarte, M. T. M. B. (1989). Impactos ambientais sobre o manguezal de Suape-PE. Acta Botanica Brasilica, 3, 09-27.
41. Fonstad, M.A., Dietrich, J.T., Courville, B.C., Jensen, J.L., Carbonneau, P.E., 2013. Topographic structure from motion: a new development in photogrammetric measurement. Earth Surf. Process. Landf. 38, 421–430. https://doi.org/10.1002/esp.3366
42. Ai, M., Hu, Q., Li, J., Wang, M., Yuan, H., & Wang, S. (2015). A robust photogrammetric processing method of low-altitude UAV images. Remote Sensing, 7(3), 2302-2333.
43. Mancini, F., Dubbini, M., Gattelli, M., Stecchi, F., Fabbri, S., & Gabbianelli, G. (2013). Using unmanned aerial vehicles (UAV) for high-resolution reconstruction of topography: The structure from motion approach on coastal environments. Remote sensing, 5(12), 6880-6898.
44. Guerra-Hernández, J., Cosenza, D. N., Rodriguez, L. C. E., Silva, M., Tomé, M., Díaz-Varela, R. A., & González-Ferreiro, E. (2018). Comparison of ALS-and UAV (SfM)-derived high-density point clouds for individual tree detection in Eucalyptus plantations. International Journal of Remote Sensing, 39(15-16), 5211-5235.
45. Jiang, S., Jiang, C., & Jiang, W. (2020). Efficient structure from motion for large-scale UAV images: A review and a comparison of SfM tools. ISPRS Journal of Photogrammetry and Remote Sensing, 167, 230-251.
46. Hossain, M. D., & Chen, D. (2019). Segmentation for Object-Based Image Analysis (OBIA): A review of algorithms and challenges from remote sensing perspective. ISPRS Journal of Photogrammetry and Remote Sensing, 150, 115-134.
47. Miraki, M., Sohrabi, H., & Immitzer, M. (2023). Tree Species Mapping in Mangrove Ecosystems Using UAV-RGB Imagery and Object-Based Image Classification. Journal of the Indian Society of Remote Sensing, 1-9.
48. Happ, P. N., Ferreira, R. S., Bentes, C., Costa, G. A. O. P., & Feitosa, R. Q. (2010). Multiresolution segmentation: a parallel approach for high resolution image segmentation in multicore architectures. The International Archives of the Photogrammetry, Remote Sensing and Spatial Information Sciences, 38(4), C7.
49. Munyati, C. (2018). Optimising multiresolution segmentation: Delineating savannah vegetation boundaries in the Kruger National Park, South Africa, using Sentinel 2 MSI imagery. International Journal of Remote Sensing, 39(18), 5997-6019.
50. Aguilar, M. A., Aguilar, F. J., García Lorca, A., Guirado, E., Betlej, M., Cichón, P., ... & Parente, C. (2016). Assessment of multiresolution segmentation for extracting greenhouses from WorldView-2 imagery. The International Archives of the Photogrammetry, Remote Sensing and Spatial Information Sciences, 41, 145-152.
51. Oliveira, P. A., Conti, L. A., Neto, F. C. N., Barcellos, R. L., & Cunha-Lignon, M. (2024). Mangrove individual tree detection based on the uncrewed aerial vehicle multispectral imagery. Remote Sensing Applications: Society and Environment, 33, 101100.
52. Haralick RM, Shanmugam K, Denstien I (1973) Textural features for image classification. IEEE Trans Syst Man Cybern 3(6):610–621

53. Ramsey, E. W. and Jensen , J. R. 1996 . Remote sensinf of mangrove wetland- Relating canopy spectra to site-specific data. Photogrammetric Engineering & Remote Sensing , 62 (8) : 939 – 948 .
54. McFeeters, S. K. (1996). The use of the Normalized Difference Water Index (NDWI) in the delineation of open water features. International journal of remote sensing, 17(7), 1425-1432.
55. Gupta, K., Mukhopadhyay, A., Giri, S., Chanda, A., Majumdar, S. D., Samanta, S., ... & Hazra, S. (2018). An index for discrimination of mangroves from non-mangroves using LANDSAT 8 OLI imagery. MethodsX, 5, 1129-1139.
56. Schaeffer-Novelli, Y., Soriano-Sierra, E. J., do Vale, C. C., Bernini, E., Rovai, A. S., Pinheiro, M. A. A., ... & Cintrón-Molero12, G. (2015). Climate changes in mangrove swamps/forests and salt marshes. BRAZILIAN JOURNAL OF OCEANOGRAPHY, 63, 00-00.
57. Blaschke, T. (2010). Object based image analysis for remote sensing. ISPRS journal of photogrammetry and remote sensing, 65(1), 2-16.
58. Haq, M. A., Rahaman, G., Baral, P., & Ghosh, A. (2021). Deep learning based supervised image classification using UAV images for forest areas classification. Journal of the Indian Society of Remote Sensing, 49, 601-606.
59. Franklin, S. E. (2018). Pixel-and object-based multispectral classification of forest tree species from small unmanned aerial vehicles. Journal of Unmanned Vehicle Systems, 6(4), 195-211.
60. Thoha, A. S., Hulu, D. L. N., Sari, T. Y., & Mardiyadi, Z. (2022). Utilization of UAV technology for mapping of mangrove ecosystem at Belawan, Medan City, North Sumatera, Indonesia. In IOP Conference Series: Earth and Environmental Science (Vol. 977, No. 1, p. 012102). IOP Publishing.
61. Zhang, K., Maskey, S., Okazawa, H., Hayashi, K., Hayashi, T., Sekiyama, A., ... & Fiwa, L. (2022). Assessment of three automated identification methods for ground object based on UAV imagery. Sustainability, 14(21), 14603.
62. Alappatt, J. P. (2008). Structure and species diversity of mangrove ecosystem. In Biodiversity and Climate Change Adaptation in Tropical Islands (pp. 127-144). Academic Press.
63. Adhikari, A., Kumar, M., & Agrawal, S. (2021). An integrated object and machine learning approach for tree canopy extraction from UAV datasets. Journal of the Indian Society of Remote Sensing, 49, 471-478
64. Osco, L. P., Junior, J. M., Ramos, A. P. M., de Castro Jorge, L. A., Fatholahi, S. N., de Andrade Silva, J., ... & Li, J. (2021). A review on deep learning in UAV remote sensing. International Journal of Applied Earth Observation and Geoinformation, 102, 102456.
65. Singh, A., Thakur, N., & Sharma, A. (2016). A review of supervised machine learning algorithms. In 2016 3rd International Conference on Computing for Sustainable Global Development (INDIACom) (pp. 1310-1315). Ieee.
66. Osisanwo, F. Y., Akinsola, J. E. T., Awodele, O., Hinmikaiye, J. O., Olakanmi, O., & Akinjobi, J. (2017). Supervised machine learning algorithms: classification and comparison. International Journal of Computer Trends and Technology (IJCTT), 48(3), 128-138
67. Franklin, J., & Miller, J. A. (2009). Mapping species distributions: spatial inference and prediction. Cambridge University Press.
68. Deneu, B., Joly, A., Bonnet, P., Servajean, M., & Munoz, F. (2022). Very high resolution species distribution modeling based on remote sensing imagery: how to capture fine-grained and large-scale vegetation ecology with convolutional neural networks?. Frontiers in plant science, 13, 839279.
69. Harris, N. L., Goldman, E., Gabris, C., Nordling, J., Minnemeyer, S., Ansari, S., ... & Potapov, P. (2017). Using spatial statistics to identify emerging hot spots of forest loss. Environmental Research Letters, 12(2), 024012.
70. Zhang, M. G., Slik, J. F., & Ma, K. P. (2016). Using species distribution modeling to delineate the botanical richness patterns and phytogeographical regions of China. Scientific reports, 6(1), 22400.
71. Wu, Y., Falconer, R. A., & Struve, J. (2001). Mathematical modelling of tidal currents in mangrove forests. Environmental Modelling & Software, 16(1), 19-29.
72. Zheng, J. Y., Hao, Y. Y., Wang, Y. C., Zhou, S. Q., Wu, W. B., Yuan, Q., ... & Zhao, B. (2022). Coastal Wetland Vegetation Classification Using Pixel-Based, Object-Based and Deep Learning Methods Based on RGB-UAV. Land, 11(11), 2039.
73. Kazemi, A., Van de Riet, K., & Curet, O. M. (2017). Hydrodynamics of mangrove-type root models: the effect of porosity, spacing ratio and flexibility. Bioinspiration & biomimetics, 12(5), 056003.
74. Conti, L. A., de Araújo, C. A. S., & Cunha-Lignon, M. (2016). Spatial database modeling for mangrove forests mapping; example of two estuarine systems in Brazil. Modeling Earth Systems and Environment, 2, 1-12.